^{1}H Resonance Assignments and Secondary Structure of the 13.6 kDa Glycosylated Adhesion Domain of Human CD2†

Daniel F. Wyss,‡,§ Jane M. Withka,‡,§ Maria H. Knoppers,∥ Kyle A. Sterne,∥ Michael A. Recny,∥ and Gerhard Wagner*,§

Department of Biological Chemistry and Molecular Pharmacology, Harvard Medical School, Boston, Massachusetts 02115 and, Procept, Inc., Cambridge, Massachusetts 02139

Received June 3, 1993; Revised Manuscript Received August 5, 1993•

ABSTRACT: Human CD2, a glycosylated transmembrane receptor found on all T-lymphocytes, plays a key role in facilitating cellular adhesion between T-cells and target cells or antigen-presenting cells by binding to its counter receptor CD58 (LFA-3) present on the surface of those cells. All CD2 adhesion functions are localized within the amino-terminal 105-residue domain, which contains a single high mannose *N*-glycan required for maintaining both the conformational stability and CD58 binding properties of the glycoprotein. In order to better understand the structural basis for CD2–CD58-mediated adhesion and the critical role of the carbohydrate moiety in maintaining the functional stability of the molecule, we have determined the secondary structure of the *N*-glycosylated adhesion domain of human CD2 (hu-sCD2$_{105}$) using NMR spectroscopy. Most of the ^{1}H resonance assignments have been obtained from ^{1}H–^{1}H homonuclear 2D NMR spectra, which were further extended by applying ^{1}H–^{15}N heteronuclear 2D experiments on a hu-sCD2$_{105}$ sample selectively labeled with [^{15}N]lysine. Thus, 98% of all backbone ^{1}H resonances and over 80% of all side chain ^{1}H resonances have been assigned. An overall topology characteristic of an immunoglobulin variable domain is observed, which consists of two β-sheets comprised of three (residues 16–20, 67–71, and 60–63) and five (residues 94–103, 80–86, 32–37, 45–47, and 53–55) antiparallel β-strands, respectively, with a hydrophobic core sandwiched between them. A ninth β-strand (residues 7–12) makes parallel contacts to the carboxy-terminal β-strand. NOEs between the *N*-linked glycan and the protein have tentatively been identified.

The ability of the immune system to detect and respond to the presentation of foreign antigens is dependent upon a distinct array of cell surface receptors that regulate both cell–cell adhesion and subsequent activation of the immune response. The initial adhesion of T-lymphocytes to target cells and antigen presenting cells (APCs)[1] in humans is mediated by CD2 (T11), an invariant 50–55-kDa transmembrane glycoprotein that regulates primary cell–cell adhesion between these cells [reviewed in Moingeon et al. (1989a) and Bierer et al. (1989)]. In humans, CD2 binds specifically to CD58 (LFA-3) present on the surface of target cells and APCs (Shaw et al., 1986; Selvaraj et al., 1987). CD2–CD58 mediated adhesion facilitates T-cell recognition of foreign antigens by enhancing contact resonance time between cells, thereby allowing for productive engagement of the T-cell receptor (TCR) with antigens presented by the major histocompatibility complex (MHC) on APCs (Bierer et al., 1988; Moingeon et al., 1989b; Koyasu et al., 1990) prior to up-regulation of other receptor-mediated adhesion pathways (Dustin & Springer, 1989; Moingeon et al., 1991). Previous studies have demonstrated that anti-CD2 monoclonal antibodies directed against a specific epitope (T11$_1$) which inhibit CD58 binding also inhibit cell–cell adhesion, leading to suppression of cellular-mediated immune responses (Meuer et al., 1984; Bierer et al., 1988). In addition, blocking CD2–CD58 interactions between T-cells and APCs with a soluble version of the human CD2 extracellular domain can also effectively suppress both memory T-cell responses to recall antigens and alloreactive responses (Rabin et al., 1993).

Human CD2 is a member of the immunoglobulin gene superfamily (Williams & Barclay, 1988; Williams et al., 1989) and consists of a two-domain 185 amino acid residue extracellular segment, a 25-residue hydrophobic transmembrane-spanning region, and a 117-residue cytoplasmic tail (Sewell et al., 1986; Sayre et al., 1987; Clayton et al., 1987) which is required for CD2-mediated signal transduction (Moingeon et al., 1989b; Chang et al., 1989). Previous studies demonstrated that all CD58 binding activity resides in the extracellular amino-terminal 105-residue domain of human CD2 (Recny et al., 1990). This immunoadhesion domain contains a single consensus *N*-glycosylation site at Asn65 that is occupied with high mannose oligosaccharides [(Man)$_n$-GlcNAc$_2$, n = 5–9] when a soluble version of the CD2 extracellular segment is expressed in Chinese hamster ovary (CHO) cells (Recny et al., 1992). Occupancy of this site with *N*-linked carbohydrates is essential for maintaining the

† This work was supported in part by a grant from the Swiss National Science Foundation to D.F.W., a NIH postdoctoral fellowship (F32-GM15646-01) to J.M.W., and a grant from Procept, Inc.

‡ D.F.W. and J.M.W. contributed equally to this work.

§ Harvard Medical School.

∥ Procept, Inc.

• Abstract published in *Advance ACS Abstracts,* October 1, 1993.

[1] Abbreviations: APC, antigen-presenting cell; CD2, cluster of differentiation 2; CHO cells, Chinese hamster ovary cells; COSY, correlated spectroscopy; DSS, sodium 2,2-dimethyl-2-silapentane sulfonate; *EASY*, ETH Automated Spectroscopy; GlcNAc, *N*-acetylglucosamine; HMQC, heteronuclear multiple-quantum correlation; Ig V domain, immunoglobulin variable domain; LFA-3, lymphocyte function-associated antigen-3; Man, mannose; MHC, major histocompatibility complex; NMR, nuclear magnetic resonance; NOESY, nuclear Overhauser enhancement spectroscopy; ppm, parts per million; r-sCD2$_{99}$, nonglycosylated adhesion domain of rat CD2; r-sCD2$_{177}$, two-domain extracellular segment of rat CD2 with the *N*-linked glycans trimmed down to monosaccharide (GlcNAc) units; SCUBA, stimulated cross peaks under bleached alphas; TCR, T-cell receptor; TOCSY, total correlation spectroscopy; hu-sCD2$_{182}$, two-domain 182 amino acid glycosylated extracellular segment of human CD2; hu-sCD2$_{105}$, amino-terminal 105 amino acid N-glycosylated adhesion domain of human CD2; τ_m, mixing time; 2D, two dimensional; 2Q, double quantum; 2QF, double quantum filtered; 3D, three dimensional.

0006-2960/93/0432-10995$04.00/0

conformational stability of the CD2 adhesion domain and its presence is required for retaining a functional CD58 binding site (Recny et al., 1992).

Recently, an NMR solution structure of the nonglycosylated domain 1 of rat CD2 (r-sCD2$_{99}$) (Driscoll et al., 1991) and the crystal structure of the entire two-domain extracellular portion of rat CD2 (r-sCD2$_{177}$) were reported (Jones et al., 1992). In the latter study, r-sCD2$_{177}$ was expressed in Chinese hamster ovary cells, but the four *N*-linked glycans were trimmed down to single GlcNAc monosaccharide units with endoglycosidase H in order to facilitate crystallization of the two-domain rat molecule. In contrast to human CD2 (Recny et al., 1992), the presence of these *N*-glycans does not appear to be required for structural stability of either the one-domain or two-domain rat CD2 receptors. Both rat CD2 structures reveal characteristic immunoglobulin-like folding patterns for each domain, which consist of two β-sheets composed of nine (domain 1) and seven (domain 2) antiparallel β-strands with a hydrophobic core sandwiched between them. There is approximately 41% overall sequence homology between the rat and human extracellular domains of CD2, and similar structural elements have been predicted for human CD2 on the basis of homologous alignment of their respective primary sequences (Killeen et al., 1988; Driscoll et al., 1991).

However, the natural ligand for both rat CD2 (Jones et al., 1992) and murine CD2 (Kato et al., 1992) has recently been shown to be CD48, known as OX-45 in rats (Killeen et al., 1988) and BCM1 in mice (Wong et al., 1990). In the human system, CD48 binds CD2 with much lower affinity ($K_d \sim 100$ μM) (Arulanandam et al., 1993) than CD58 ($K_d \sim 1$ μM) (Sayre et al., 1989; Recny et al., 1990). Thus, although CD48 is structurally homologous to CD58, the role of CD48 in mediating cell–cell adhesion may be of little, if any, physiological significance in humans. In addition, there have been reports suggesting that CD59 is an alternative ligand for human CD2 whose binding site overlaps with CD58 (Hahn et al., 1992; Deckert et al., 1992), but other evidence directly contradicts these findings (Arulanandam et al., 1993).

Therefore, since the physiological ligands for rodent CD2 and human CD2 have apparently diverged through evolution and the human CD2 adhesion domain clearly requires the presence of the *N*-linked oligosaccharide for maintaining both structural stability and functional CD58 binding properties, we initiated the investigation of the solution structure of the glycosylated adhesion domain of human CD2 by NMR spectroscopy in order to better understand the structural aspects that regulate human CD2 adhesion functions.

Here we report the sequential ^{1}H NMR assignments of hu-sCD2$_{105}$ obtained primarily by homonuclear 2D NMR experiments. In addition, a sample selectively labeled with [^{15}N]lysine was used to facilitate the assignments of the 20 lysine residues in hu-sCD2$_{105}$ using various heteronuclear experiments. Complete backbone ^{1}H resonance assignments have been achieved for 102 out of the 105 residues within this glycosylated domain. The three residues for which unambiguous backbone assignments are still missing lie in an apparently more flexible region. Secondary structure elements have been derived on the basis of the NMR data, and the tertiary fold has been characterized. These assignments lay the groundwork necessary for a detailed characterization of the three-dimensional solution structure and dynamics of hu-sCD2$_{105}$. The assignments and conformational studies of the *N*-linked oligosaccharide were hampered due to variable branching within the high mannose glycomer, and sequential assignments have not been obtained so far. However, we have tentatively identified two NOEs which define contacts between the high mannose oligosaccharide and one amino acid residue.

EXPERIMENTAL PROCEDURES

Protein Expression, Purification, and Sample Preparation. Methods for the construction of mammalian cell expression vectors coding for secretion of a soluble version of two-domain hu-sCD2$_{182}$ receptor in CHO cells, purification of hu-sCD2$_{182}$, and production of one-domain hu-sCD2$_{105}$ from clostripain digestion of hu-sCD2$_{182}$ have been described in detail elsewhere (Recny et al., 1992). High-producing hu-sCD2$_{182}$ CHO cell clones (>10 mg/L) maintained in 1 μM methotrexate were seeded in 8-L spinner vessels (10^5 cells/mL) with 8 gm/L CYTODEX 3 microcarriers (Sigma) and grown in alpha-MEM (purchased from Fischer Scientific and Mediatech) containing 6 mM glutamine, 4 gm/L glucose, 10% fetal calf serum, and 1 μM methotrexate. Cultures were maintained at 37 °C with replacement of the medium every 3 days. In order to ensure that purity was optimal, the adhesion domain was repurified by immunoaffinity chromatography on an anti-CD2 mAb column prior to size exclusion chromatography. Hu-sCD2$_{182}$ selectively enriched for [^{15}N]lysine was obtained by replacing the unlabeled lysine in the alpha MEM with pure, crystalline [^{15}N]lysine purchased from Cambridge Isotope Research Laboratories (Woburn, MA). Two 8-L suspension cultures were grown in the presence of [^{15}N]lysine supplemented alpha-MEM medium for 3 days prior to harvesting, when the medium was replaced in one of the spinners and second labeling was performed. During the production phase for [^{15}N]lysine-labeled hu-sCD2$_{182}$, the methotrexate was removed from the media, the fetal calf serum was raised to 15%, and 0.1 gm/L pluronic F68 was added. [^{15}N]lysine labeled hu-sCD2$_{105}$ was prepared from the two-domain molecule as described (Recny et al., 1992). Samples (1.0–1.5 mM) were prepared for NMR experiments by dialysis into 20 mM deuterated acetate buffer, pH 4.5.

NMR Spectroscopy. All NMR experiments were performed in 95% (v/v) H_2O/D_2O or D_2O. Acquired 2D ^{1}H–^{1}H NMR data included 2Q-COSY (Braunschweiler et al., 1983; Wagner & Zuiderweg, 1983), 2QF-COSY (Piantini et al., 1982; Shaka & Freeman, 1983; Rance et al., 1983), TOCSY (Braunschweiler & Ernst, 1983), and NOESY (Jeener et al., 1979; Anil-Kumar et al., 1980). Experiments were carried out either on Bruker AMX600 or AMX500 spectrometers with ^{1}H resonance frequencies of 600.13 and 500.13 MHz, respectively. While most experiments were carried out at 25 °C, some spectra were recorded at 13 and 37 °C to resolve accidental overlaps. All the data shown here refer to the experiments at 25 °C, unless otherwise stated. All spectra were recorded in a phase-sensitive manner using the time-proportional phase incrementation method for sign discrimination in the F_1 dimension (Marion & Wüthrich, 1983). Spectral widths in the ^{1}H dimension(s) were 8772 and 7246 Hz for the AMX600 and AMX500 spectrometer, respectively. Typically, the spectra were obtained with 512 real points along t_1 (TPPI) and 2048 complex points along t_2. ^{1}H chemical shifts (δ) were referenced relative to the water resonance, calibrated in turn at 4.631, 4.755, and 4.879 ppm at 37, 25, 13 °C, respectively, on an external DSS standard. The ^{1}H carrier was placed on the H_2O or residual DHO resonance. The water resonance was suppressed by low-power presaturation during the recycle delay (1.0–1.3 s) followed by the SCUBA sequence using 30 ms delays to recover saturated proton resonances under the water line (Brown et al., 1988). For the NOESY experiments, solvent peak recovery was

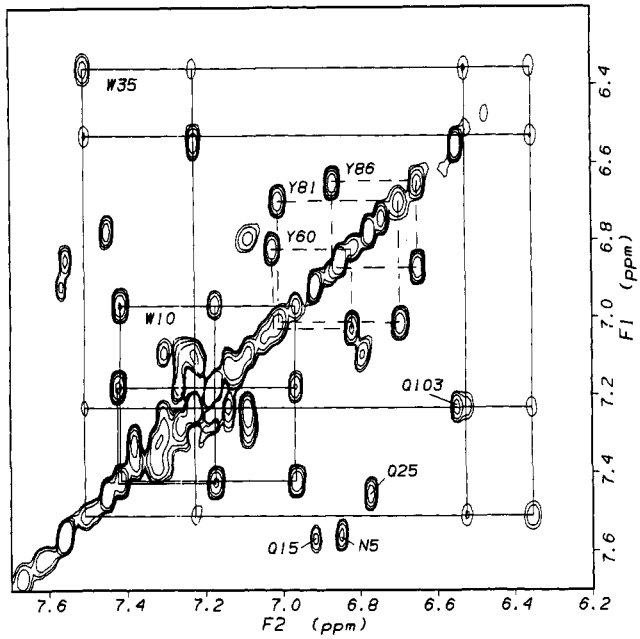

FIGURE 1: Aromatic region of a TOCSY spectrum of hu-sCD2$_{105}$, recorded in H_2O at 25 °C, pH 4.5, with three mixing times of 32, 55, and 85 ms coadded to a single file. The spin systems of the two Trp residues are indicated by solid lines. The $C^{2,6}H/C^{3,5}H$ cross peaks of the three Tyr residues are marked by dashed lines. Cross peaks from the side chain amide protons of Asn5, Gln15, Gln25 and Gln103 are also indicated below the diagonal. The residual unmarked cross peaks in this region result from the five Phe residues.

reduced by inclusion of a 180° composite pulse in the center of the mixing period, and mixing times (τ_m) of 38, 76, 100, and 200 ms were used. A total of 512 t_1 values were collected per mixing time with 256 scans acquired for each t_1 value. All TOCSY spectra were acquired using the DIPSI-II (Shaka et al., 1988) spin-locking sequence. They were either recorded with three different mixing times of 32, 55, and 85 ms, which were coadded to a single file, or they were acquired with single short mixing times of 12, 22, and 32 ms, respectively. A total of 512 t_1 values were collected per mixing time with 72 scans acquired for each t_1 value.

Because of the unusual high content of Lys residues in hu-sCD2$_{105}$ (20/105 residues), a 2D ^{15}N–^1H HMQC (Mueller, 1979) and 2D $^{15}N(\omega_2)$-half-filtered TOCSY and NOESY (Otting et al., 1986; Otting & Wüthrich, 1990) spectra were recorded at 25 °C on a submillimolar sample selectively labeled with ^{15}N at all lysine positions to assist in the resonance assignments. On the AMX600 spectrometer with a ^{15}N frequency of 60.81 MHz, the ^{15}N spectral width was set to 8772 Hz centered around the carrier position at 116 ppm relative to liquid ammonia. The GARP sequence was used for ^{15}N decoupling during ^1H acquisition. In the half-filtered experiments, ^{15}N decoupling during t_1 was achieved through a 180° ^{15}N pulse in the middle of t_1. The isotope-filter delay was 5.5 ms. For the HMQC spectrum, 256 t_1 values were collected with eight scans acquired for each t_1 value, and for the TOCSY and NOESY spectra 512 t_1 values were collected with 128 and 256 scans acquired for each t_1 value, respectively. The mixing times for the TOCSY and NOESY measurements were 48 and 76 ms, respectively.

Data were processed either on a Sun Sparcstation 2 or on a Silicon Graphics 4D/35 Personal Iris computer using Felix software (Hare Research, Inc.). If necessary, low-frequency deconvolution (Marion et al., 1989) was applied to the acquisition dimension to remove the water signal. Typically, the data were zero-filled once in the t_1 dimension and

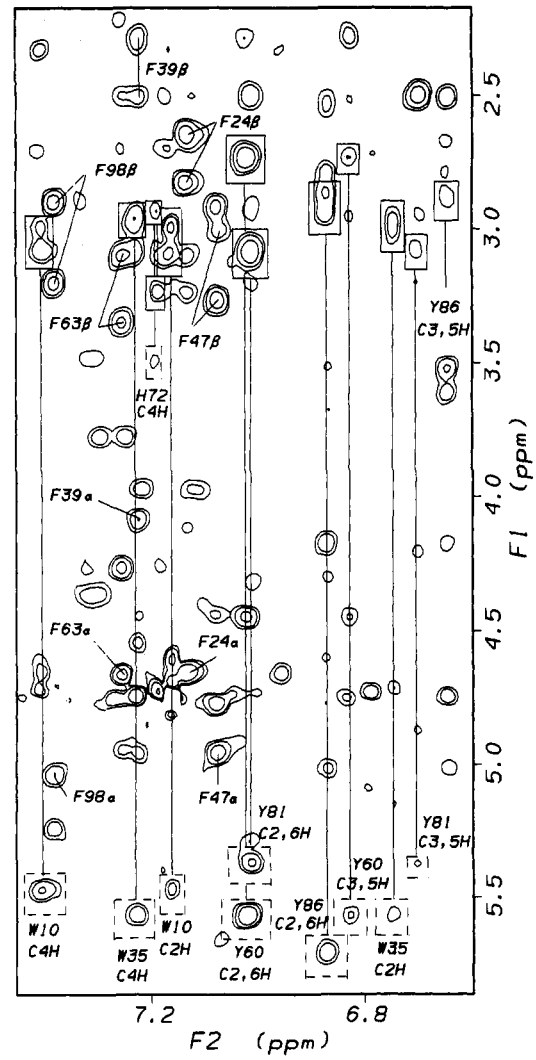

FIGURE 2: Part of a NOESY spectrum of hu-sCD2$_{105}$, recorded in D_2O at 25 °C, pH 4.5, with a mixing time of 76 ms, showing connectivities between aliphatic and aromatic resonances for all His, Phe, Trp, and Tyr residues. For His, Trp, and Tyr residues intraresidue cross peaks to $C^\alpha H$ and $C^\beta H$ are indicated by dashed and solid boxes, respectively, and vertical lines mark the position of the aromatic resonances that are indicated together with the residue type and residue number. For the five Phe residues the $C^{2,6}H/C^\beta H$ and $C^{2,6}H/C^\alpha H$ NOEs are labeled with the residue type and residue number followed by β and α, respectively.

multiplied with a $\pi/3$, $\pi/4$, or $\pi/5$ shifted squared sine bell apodization function in both dimensions prior to Fourier transformation. A polynomial baseline correction was systematically applied to the rows of the transformed matrices. If necessary, an additional baseline correction program was applied to the frequency domain data (Chylla & Markley, 1993). Data were analyzed with the EASY program package (Eccles et al., 1991).

RESULTS

Most of the ^1H resonance assignments for hu-sCD2$_{105}$ were achieved following standard homonuclear 2D NMR procedures (Wagner & Wüthrich, 1982; Wüthrich, 1986). In the first step, NMR resonances were associated with spin systems arising from the different types of amino acids of hu-sCD2$_{105}$ through intraresidue through-bond connectivities obtained in 2QF-COSY, 2Q, and TOCSY spectra. In a second phase, these spin systems were allocated to specific positions in the amino acid sequence by establishing sequential interresidue through-space (<5 Å) connectivities obtained from NOESY

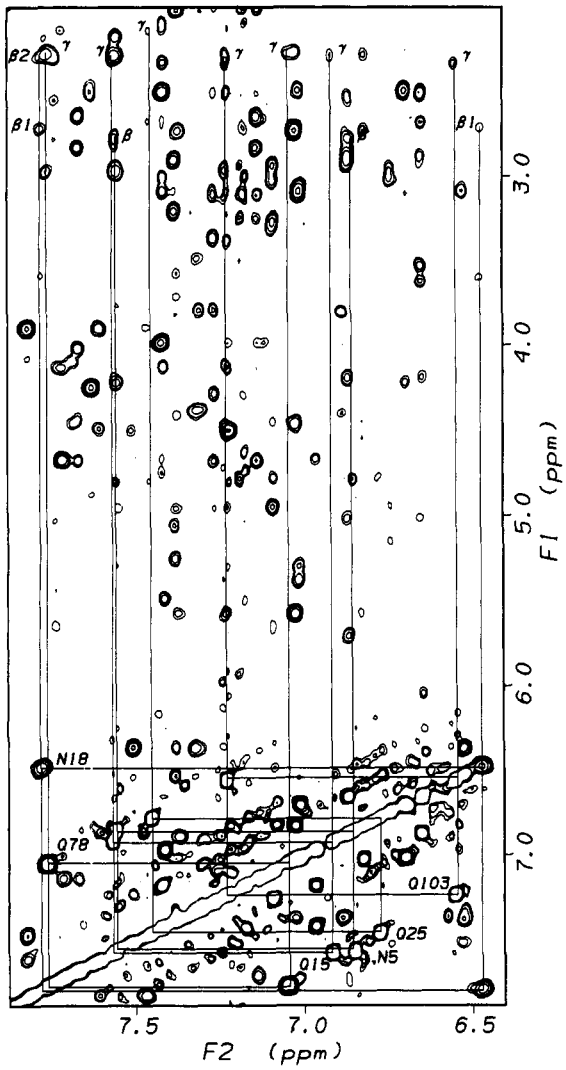

FIGURE 3: Part of a NOESY spectrum of hu-sCD2$_{105}$, recorded in H_2O at 25 °C, pH 4.5, with a mixing time of 100 ms, showing the assignment of two of the four Asn and four of the five Gln spin systems. The connectivities between aliphatic and amide side chain protons are indicated by continuous lines.

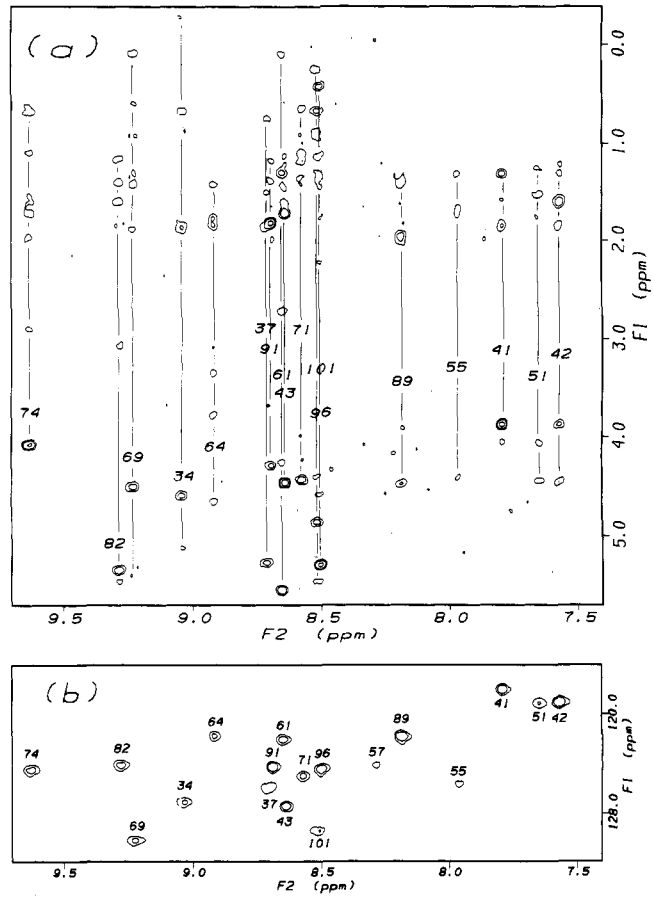

FIGURE 4: (a) Fingerprint region of a 2D $^{15}N(\omega_2)$-half-filtered NOESY spectrum, acquired with a mixing time of 76 ms and (b) part of a ^{15}N–^1H HMQC spectrum of hu-sCD2$_{105}$, showing the assignment of Lys residues. Both spectra were recorded in H_2O at 25 °C, pH 4.5. The NH positions of the Lys residues are indicated with the respective residue number. For Lys57 no cross peaks were observed in the $^{15}N(\omega_2)$-half-filtered NOESY spectrum.

spectra. Hu-sCD2$_{105}$ contains an unusually large number of Lys residues (20 out of 105). In order to facilitate assignments a sample was prepared in CHO cells whereby all lysine residues were selectively labeled with [^{15}N]lysine. The program package, EASY (for ETH Automated Spectroscopy) (Eccles et al., 1991), was interactively used for all steps in the assignment process. This computer-supported assignment procedure was invaluable due to resonance overlap in the homonuclear 2D spectra. Most of the resonance assignments were achieved by analyzing spectra recorded at 25 °C and pH 4.5. In order to recognize spin systems whose C$^\alpha$H resonances were bleached due to the irradiation of the water resonance at 25 °C, additional spectra at 13 and 37 °C were obtained. Thus, the assignments at 25 °C were verified and extended.

Spin System Identification. Spin system assignments were initiated by analyzing the fingerprint region of a 2QF-COSY and a TOCSY spectrum recorded at 25 °C in H_2O. The COSY spectrum was used to distinguish between direct (three-bond) peaks and more remote (relay) peaks. In addition, a 2Q spectrum obtained at 25 °C helped to identify the NH–CH three-bond connectivities through direct cross peaks located at positions [(NH+CH)ω_1,(NH)ω_2]. Six NH–CH three-bond connectivities could easily be associated with three of the four Gly residues of hu-sCD2$_{105}$, as was determined by the corresponding remote cross peaks located at positions [(C$^\alpha$H+C$^\alpha$H)ω_1,(NH)ω_2] in the 2Q spectrum.

Subsequently, the high-field regions were analyzed with 2QF-COSY and TOCSY spectra recorded in D_2O at 25 °C and with an additional TOCSY spectrum recorded in D_2O at 37 °C. Thus, it was possible to unambiguously connect 85 side chain spin systems to their NH/C$^\alpha$H cross peaks and to extend most of the 76 spin systems for which at least one relayed connectivity from the NH to a side chain proton resonance had previously been observed in the fingerprint regions of the TOCSY spectra recorded in H_2O. The identified and extended spin systems were classified into specific spin system types and residues when possible.

Analysis of NOESY spectra recorded at 25 and 37 °C, both in H_2O and in D_2O, allowed determination of the residue type of all 11 aromatic residues of hu-sCD2$_{105}$. Complete spin system networks for the C^{4}H, C^{5}H, C^{6}H, and C^{7}H ring protons from the two tryptophans, as well as for the C^{2,6}H, and C^{3,5}H ring protons from the three tyrosines were readily identified in TOCSY spectra and are illustrated in Figure 1. All tyrosyl side chains are rotating rapidly on the NMR time scale and show averaged resonances for the δ and ϵ ^1H resonances, respectively. Two further cross peaks linking the imidazole N^{1}H and the C^{2}H ring protons of the two Trp residues and a cross peak linking the C^{2}H and the C^{4}H ring protons of the single histidine were also observed in TOCSY spectra (not shown). The links between these aromatic spin systems and their corresponding AMX spin systems were

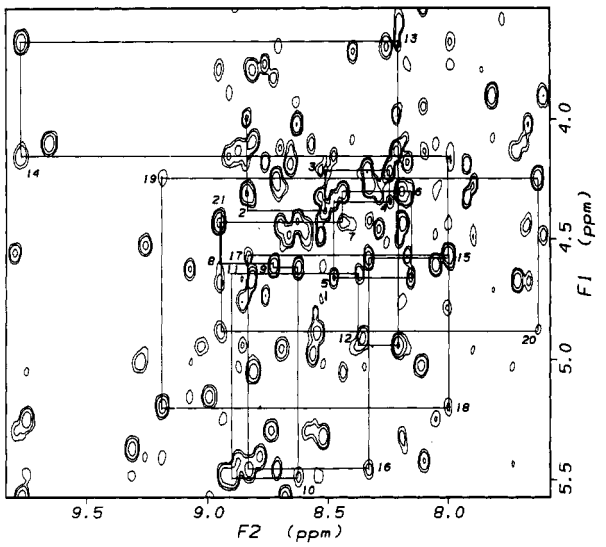

FIGURE 5: Part of the fingerprint region of the same spectrum as in Figure 3. Sequential $d_{\alpha N}(i,i+1)$ connectivity pathways are indicated for residues 1–21. Note that intraresidue NH/C$^{\alpha}$H NOEs are not seen for all residues. The numbers indicate the residue position in the sequence.

established through NOESY cross peaks shown in Figure 2. Because of overlap, the aromatic spin systems of the five Phe residues could only partially be assigned. However, in NOESY spectra intraresidue cross peaks from the C^{2,6}H ring protons to the C$^{\beta}$H$_2$ and C$^{\alpha}$H resonances were observed for all five phenylalanines (see Figure 2). These links were confirmed through additional intraresidue C^{2,6}H/NH NOEs detected in NOESY spectra with longer mixing times (τ_m = 100 ms) (not shown). The C$^{\beta}$H$_2$ resonances for two of the four asparagines and the C$^{\gamma}$H$_2$ resonances for four of the five glutamines were identified from NOE connectivities with their respective side chain amide protons (see Figure 3).

Spin systems of 17 of the 20 lysines were unambiguously identified through ^{15}N–^{1}H HMQC, ^{15}N(ω_2)-half-filtered TOCSY and ^{15}N(ω_2)-half-filtered NOESY spectra recorded on a selectively labeled [^{15}N]Lys hu-sCD2$_{105}$ sample at 25 °C as shown in Figure 4a,b. No cross peaks from the amino-terminal lysine were observed as its amino protons are in fast exchange with the preirradiated water resonances under the conditions measured.

Sequential Assignments. Sequence-specific resonance assignments were accomplished primarily by establishing sequential $d_{\alpha N}(i,i+1)$, $d_{NN}(i,i+1)$, and $d_{\beta N}(i,i+1)$ [in case of Ile, Thr, and Val also $d_{\gamma N}(i,i+1)$] NOESY connectivities. Examples of NOESY spectra showing sequential $d_{\alpha N}(i,i+1)$ connectivity pathways of many residues are given in Figure 5 and in the supplementary material. Except for Arg48, Glu56, and Lys57, ambiguities or interruptions in the $d_{\alpha N}(i,i+1)$ connectivity pattern could be bypassed by referring to additional sequential, medium, and long range NOEs. In this manner, oligopeptide segments were built up and matched with the known sequence of hu-sCD2$_{105}$. For several residues the side chain assignments could unambiguously be determined using NOEs only after their residue type was known from the sequence-specific assignments. For others, such as Leu62, the side chain assignments could only be completed by referring to initial model structures of hu-sCD2$_{105}$.

The sequence-specific assignment of the amino-terminal region was readily obtained through a series of consecutive C$^{\alpha}$H(i)/NH(i+1) NOEs (see Figure 5), interrupted by Pro22, as expected. The resonances of Pro22 were recognized through sequential C$^{\alpha}$H(21)/C$^{\delta}$H(22), C$^{\gamma}$H$_3$(21)/C$^{\delta}$H(22), C$^{\alpha}$H-(22)/NH(23), C$^{\beta}$H(22)/NH(23), and C$^{\gamma}$(22)/NH(23) NOEs, as well as through several intraresidue TOCSY and NOESY cross peaks (not shown). The assignment of the amino-terminal region identified an AX spin system as Gly11, the only glycine that did not show a remote peak in the 2Q

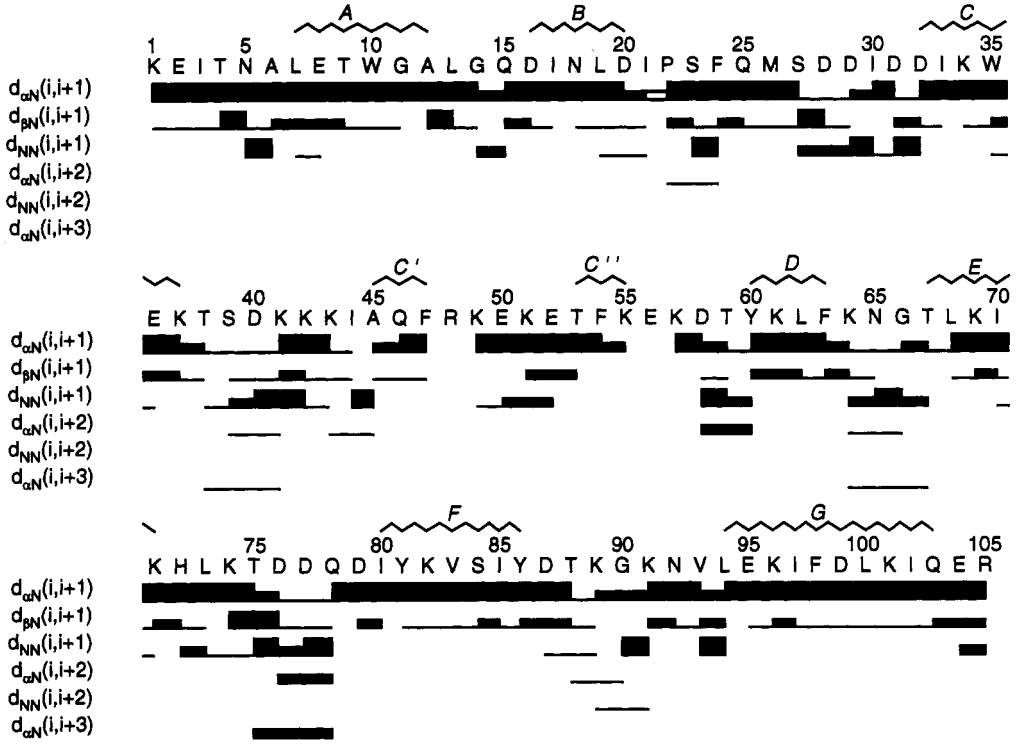

FIGURE 6: Sequence of hu-sCD2$_{105}$, together with a summary of sequential NOEs used in the sequential assignment procedure. Medium-range NOEs between backbone atoms are also included. The C$^{\alpha}$H(i)–C$^{\delta}$H(i+1) NOE is shown as an open box along the same line as the C$^{\alpha}$H-(i)–NH(i+1) connectivities. NOEs estimated to be strong, medium, and weak are distinguished by thick, medium, and thin solid horizontal bars between residues. The zigzag lines above the residue name and number indicate the position of the observed β-strands based on typical interstrand NOEs expected in regular β-sheets. The β-strands are labeled according to an Ig V domain.

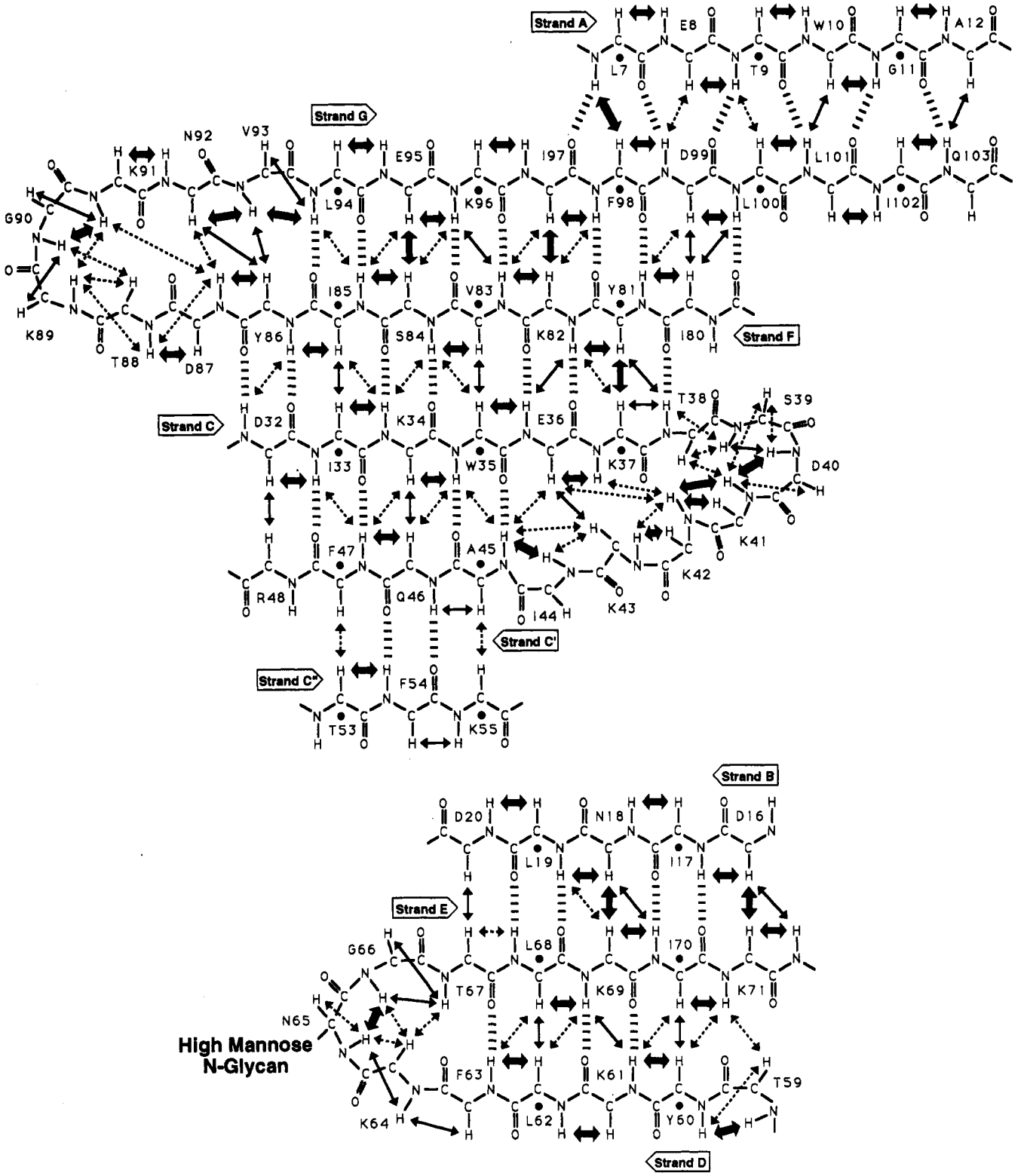

FIGURE 7: Schematic diagram illustrating NOE connectivities within and between (a, top) β-strands A, G, F, C, C′, and C″and (b, bottom) β-strands B, E, and D. The β-strands are labeled according to an Ig V domain. NOEs estimated to be strong, medium, and weak are distinguished by thick, thin, and dashed double-headed arrows, respectively. Broken lines indicate hydrogen bonds typically found in regular β-strands. Dots close to the one-letter codes and residue numbers indicate β-strand residues with the side chains pointing toward the neighboring β-sheet.

spectrum. The accidental overlap of the $C^{\alpha}H(8)/NH(9)$ and $NH(9)/C^{\alpha}H(9)$ NOEs at 25 °C was removed at 13 °C, confirming the Glu8–Thr9 connection.

^1H resonances within the two segments from Ser23 to Lys37 and Lys58 to Arg105 were relatively straightforward to assign. Their sequence-specific assignments are described in detail in the supplementary material. On the other hand, the sequential assignment of parts of the segment Thr38–Lys57 proved to be significantly more difficult than that of the other regions of hu-$sCD2_{105}$, mainly because of weak or missing NOEs. A likely reason for the weak NOE signals is substantial local mobility of residues or conformational disorder in these parts of the molecule. However, by carefully examining the sequential NOE information available in NOESY spectra recorded at different temperatures (13 , 25, and 37 °C) and frequencies (500 and 600 MHz), it was possible to trace all

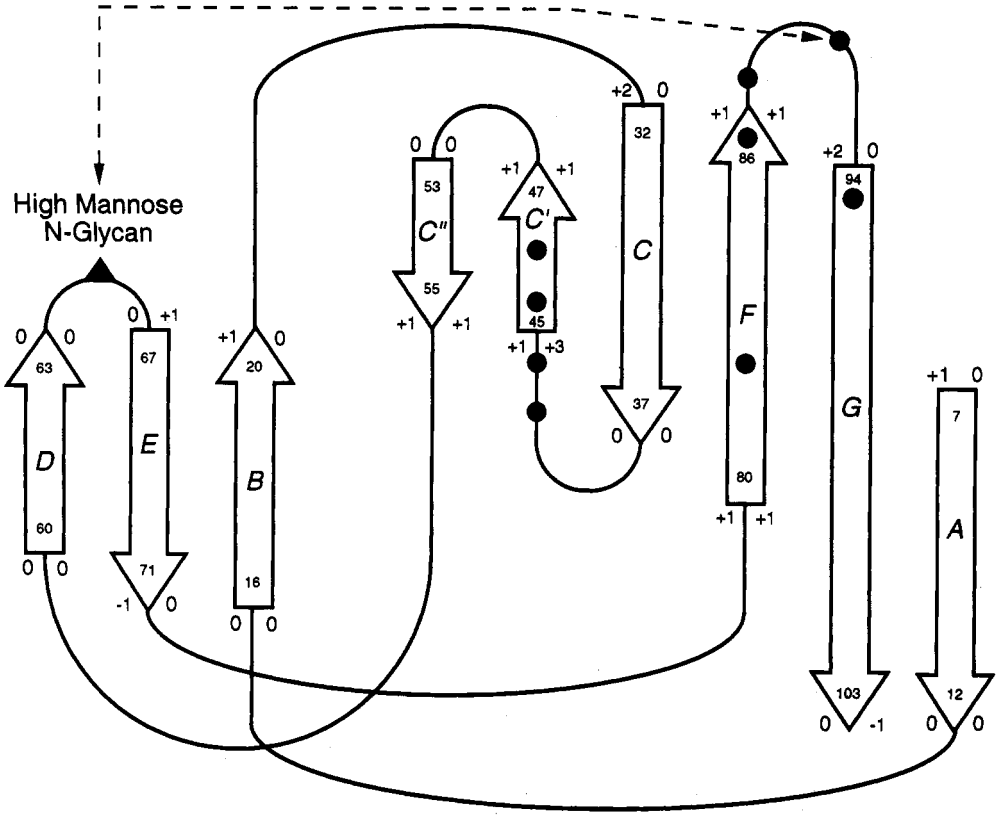

FIGURE 8: Schematic diagram showing the topology of β-strand connections in hu-sCD2$_{105}$. Open arrows represent β-strands labeled A–G according to an Ig V domain. NOEs between side chain resonances of residues of the two β-sheets suggest that the BED sheet is situated above the GFCC′ strands of the other sheet. The filled triangle in the D–E loop represents the single glycosylation site at Asn65 of hu-sCD2$_{105}$. NOEs tentatively observed between the high mannose oligosaccharides and Gly90 are indicated by the dashed double-headed arrow. The positions of residues found to affect CD58 binding are indicated by filled dots. Differences between the boundaries of β-strands in r-sCD2$_{99}$ and r-sCD2$_{177}$ with respect to hu-sCD2$_{105}$ are indicated to the left or to the right (relative to the direction of the arrow) of each β-strand for r-sCD2$_{99}$ and r-sCD2$_{177}$, respectively, and are discussed in the text. For each β-strand in hu-sCD2$_{105}$ the first and last residue are indicated by its position in the sequence.

connectivities except those for Arg48, Glu56, and Lys57 (see the supplementary material).

The sequential and medium range NOEs involving NH, C$^{\alpha}$H, and C$^{\beta}$H as well as the C$^{\delta}$H of proline are summarized in Figure 6. Qualitative interpretation of these data together with observed long-range NOEs allowed the determination of the secondary structure of hu-sCD2$_{105}$ that is depicted schematically in Figures 7and 8. As presented here, the extent of each strand was defined by the observation or absence, respectively, of interstrand and sequential NOEs characteristic for regular β-strand structures. The boundaries of the strands as given in Figure 8 are thus well defined for all strands, except for the C′ and C″strands which might be longer at either end. This ambiguity is due to the incomplete assignments of Arg48, Glu56, and Lys57 (see Table I). A complete list of the proton assignments for hu-sCD2$_{105}$ obtained in this work at 25 °C is given in Table I.

Identification of Secondary Structure and Global Fold. Regular secondary structural features in protein structures can be identified by distinctive NOE patterns (Wüthrich, 1986; Wagner, 1990). β-sheet structures generally lead to strong consecutive C$^{\alpha}$H(i)/NH(i+1) NOEs, very weak or nonexistent NH(i)/NH(i+1) NOEs, and very characteristic long-range interstrand NOEs. In addition to the medium to weak NH(i+1)/C$^{\alpha}$H(j) and NH(i+1)/NH(j−1) NOEs that are also observed in parallel β-sheets, the antiparallel strand orientations are distinguishable by a series of strong C$^{\alpha}$H(i)/C$^{\alpha}$H(j) NOEs. Significant downfield NH chemical shifts and slow NH proton exchange with solvent are also common features of β-sheets, due to the networked hydrogen-bonding patterns present. In hu-sCD2$_{105}$, these characteristics of β-sheet structures were extensively observed. The results are consistent with nine β-strands organized into two mainly antiparallel β-sheets forming a topology reminiscent of an Ig variable (V) domain (see Figure 8). In the loops and turns connecting the nine β-strands these regular NOE patterns were interrupted through often much weaker sequential C$^{\alpha}$H(i)/NH(i+1) and stronger NH(i)/NH(i+1) NOEs, as well as through medium range NOEs typically observed in turns.

Figure 7a shows contacts between strands G, F, C, C′, and C″, which imply a five-stranded antiparallel β-sheet comprising residues Leu94–Gln103, Ile80–Tyr86, Asp32–Lys37, Ala45–Phe47, and Thr53–Lys55, respectively. Although a medium C$^{\alpha}$H(32)/C$^{\alpha}$H(48) NOE has been observed, Arg48 has not been included as a β-strand residue in Figures 6 and 8, because neither intraresidue nor sequential cross peaks have been observed for this residue. NOEs revealing parallel proximities between residues 7 and 12 of strand A, and residues 98 and 103 of strand G are also indicated. A strong sequential NH(5)/NH(6) NOE was observed between Asn5 and Ala6, and residues 1–5 seem to adopt an extended conformation but do not show any interstrand NOEs. These data imply that a bend occurs at this position and that the amino-terminus is pointing away from the G strand. In addition, these five amino-terminal residues showed significantly reduced NOE intensities with increasing temperature suggesting higher mobility in this part of the molecule. In Figure 7b interstrand NOEs between strands B, E, and D indicate a three-stranded antiparallel β-sheet involving segments Asp16–Asp20, Thr67–Lys71, and Tyr60–Phe63, respectively.

Table I: Chemical Shifts of the Assigned Proton NMR Resonances of hu-sCD2$_{105}$ at 25 °C, pH 4.5[a]

residue		NH	C$^{\alpha}$H	C$^{\beta}$H	others[b,c]
Lys	1		4.00	1.88	C$^{\gamma}$H$_2$ 1.43; C$^{\delta}$H$_2$ 1.69; C$^{\epsilon}$H$_2$ 2.99
Glu	2	8.83	4.39	2.02, 1.92	C$^{\gamma}$H$_2$ 2.28
Ile	3	8.51	4.22	1.85	C$^{\gamma}$H$_3$ 0.89; C$^{\gamma}$H$_2$ 1.19; C$^{\delta}$H$_3$ 0.84
Thr	4	8.24	4.34	4.16	C$^{\gamma}$H$_3$ 1.16
Asn	5	8.47	4.66	2.83, 2.78	N$^{\delta}$H$_2$ 7.55, 6.85
Ala	6	8.15	4.31	1.20	
Leu	7	8.44	4.43	1.44	C$^{\gamma}$H 1.51; C$^{\delta}$H$_3$ 0.88, 0.72
Glu	8	8.95	4.61	2.10, 1.96	C$^{\gamma}$H$_2$ 2.23
Thr	9	8.72	4.62	3.83	C$^{\gamma}$H$_3$ 1.19
Trp	10	8.62	5.49	3.09, 3.02	N^{1}H 10.19; C^{2}H 7.18; C^{4}H 7.41; C^{5}H 6.97; C^{6}H 7.18; C^{7}H 7.43
Gly	11	8.89	4.53, 3.21		
Ala	12	8.37	4.94	1.27	
Leu	13	8.21	3.68	1.57, 1.50	C$^{\gamma}$H 1.61; C$^{\delta}$H$_3$ 0.96, 0.88
Gly	14	9.76	4.16, 3.07		
Gln	15	7.99	4.59	2.17	C$^{\gamma}$H$_2$ 2.32; N$^{\epsilon}$H$_2$ 7.57, 6.92
Asp	16	8.33	5.46	2.61, 2.37	
Ile	17	8.83	4.56	1.65	C$^{\gamma}$H$_3$ 0.75
Asn	18	8.00	5.20	2.72, 2.31	N$^{\delta}$H$_2$ 7.77, 6.47
Leu	19	9.18	4.25	1.32, 1.29	C$^{\gamma}$H 1.07; C$^{\delta}$H$_3$ 0.41, 0.07
Asp	20	7.63	4.88	2.52, 2.46	
Ile	21	8.95	4.37	1.94	C$^{\gamma}$H$_3$ 0.69
Pro	22		4.43	2.34, 1.93	C$^{\gamma}$H$_2$ 2.04; C$^{\delta}$H$_2$ 3.49
Ser	23	8.63	4.02	3.94	
Phe	24	7.66	4.67	2.84, 2.66	C^{2,6}H 7.14; 7.21*; 7.10*
Gln	25	7.71	4.14	1.79, 1.70	C$^{\gamma}$H$_2$ 2.15; N$^{\epsilon}$H$_2$ 7.45, 6.77
Met	26	8.21	3.99	1.90, 1.84	C$^{\gamma}$H$_2$ 2.68, 2.52
Ser	27	7.42	[4.71]	4.09, 3.76	
Asp	28	8.83	4.30	2.75, 2.68	
Asp	29	8.19	(4.72)	2.83, 2.66	
Ile	30	7.41	4.13	2.51	C$^{\gamma}$H$_3$ 1.01
Asp	31	8.87	5.04	2.33, 2.28	
Asp	32	7.73	5.64	2.79, 2.57	
Ile	33	8.95	4.62	1.82	C$^{\gamma}$H$_3$ 0.70
Lys	34	9.07	5.15	1.91, 1.87	C$^{\gamma}$H$_2$ 1.29; 1.63; 1.46
Trp	35	8.99	5.57	3.00, 2.96	N^{1}H 9.58; C^{2}H 6.74; C^{4}H 7.23; C^{5}H 6.53; C^{6}H 6.36; C^{7}H 7.51
Glu	36	9.76	5.30	1.87	1.91
Lys	37	8.74	4.34	1.93*	
Thr	38	8.18	4.08	4.31*	C$^{\gamma}$H$_3$ 1.20
Ser	39	8.91	4.15	3.89, 4.07*	
Asp	40	7.47	[4.71]	2.68, 2.62	
Lys	41	7.82	3.90	1.91, 1.87	C$^{\gamma}$H$_2$ 1.35; 0.93*
Lys	42	7.60	4.49	1.66	
Lys	43	8.66	4.49	1.75	
Ile	44	8.59	4.26		
Ala	45	7.54	4.95	1.31	
Gln	46	9.03	5.70	2.10, 2.05	C$^{\gamma}$H$_2$ 2.61
Phe	47	9.37	4.94	3.31, 3.03	C^{2,6}H 7.09; 7.26*; 7.31*
Arg	48		(4.79)*		
Lys	49	7.86	3.79	2.04, 1.97	
Glu	50	8.80	4.10	2.29, 2.07	C$^{\gamma}$H$_2$ 2.23
Lys	51	7.68	4.46	1.79, 1.58	C$^{\gamma}$H$_2$ 1.28
Glu	52	8.29	4.32	1.99	C$^{\gamma}$H$_2$ 2.35, 2.29
Thr	53	8.53	4.44	4.21	C$^{\gamma}$H$_3$ 1.23
Phe	54	8.69	4.12	2.52, 2.29	C^{2,6}H 7.23; 7.09*
Lys	55	8.00	4.45		
Glu	56				
Lys	57	8.29*	4.49*		
Asp	58	8.53	4.40	2.73, 2.66	
Thr	59	6.89	3.81	4.02	C$^{\gamma}$H$_3$ 0.94
Tyr	60	7.36	5.57	2.75	C^{2,6}H 7.02; C^{3,5}H 6.82
Lys	61	8.68	4.29	1.33	
Leu	62	8.32	4.96	1.82, 1.40	C$^{\gamma}$H 1.02; C$^{\delta}$H$_3$ 0.81, 0.51
Phe	63	8.69	4.67	3.37, 3.11	C^{2,6}H 7.26; 7.17*
Lys	64	8.95	3.79	1.88, 1.80	C$^{\gamma}$H$_2$ 1.45
Asn	65	7.22	4.50	3.39, 2.75	N$^{\delta}$H 8.39
Gly	66	8.32	4.41, 3.46		
Thr	67	7.89	4.49	4.28	C$^{\gamma}$H$_3$ 0.97
Leu	68	8.58	4.53	0.09, −1.01	C$^{\gamma}$H 0.62; C$^{\delta}$H$_3$ 0.13, −0.23
Lys	69	9.25	5.40	1.46	
Ile	70	8.78	4.46	1.47	C$^{\gamma}$H$_3$ 0.68; C$^{\gamma}$H$_2$ 1.20, 0.60; C$^{\delta}$H$_3$ 0.17
Lys	71	8.59	4.25	1.39	1.12
His	72	8.71	3.50	3.25, 2.95	C^{2}H 8.56; C^{4}H 7.19
Leu	73	8.57	4.10	1.12	C$^{\gamma}$H 1.87; C$^{\delta}$H$_3$ 0.72, 0.65
Lys	74	9.65	(4.73)	2.01, 1.75	C$^{\gamma}$H$_2$ 1.66
Thr	75	8.76	3.77	4.18	C$^{\gamma}$H$_3$ 1.31

Table I (Continued)

residue		NH	$C^{\alpha}H$	$C^{\beta}H$	others[b,c]
Asp	76	8.17	4.58	2.67	
Asp	77	7.99	4.63	2.93, 2.54	
Gln	78	7.55	4.22	2.19	$C^{\gamma}H_2$ 2.29; $N^{\epsilon}H_2$ 7.76, 7.05
Asp	79	8.34	4.56	2.51, 1.93	
Ile	80	9.79	5.30	1.66	$C^{\gamma}H_3$ 0.82; $C^{\gamma}H_2$ 1.08
Tyr	81	9.90	5.38	3.10, 3.06	$C^{2,6}H$ 7.01; $C^{3,5}H$ 6.70
Lys	82	9.31	5.48	1.63	$C^{\gamma}H_2$ 1.19; $C^{\delta}H_2$ 1.44; $C^{\epsilon}H_2$ 2.66
Val	83	8.93	4.90	−0.84	$C^{\gamma}H_3$ 0.45, −0.26
Ser	84	8.35	5.03	3.63, 3.54	
Ile	85	8.11	5.00	1.47	$C^{\gamma}H_3$ 0.86; $C^{\gamma}H_2$ 0.91
Tyr	86	9.28	5.70	2.93, 2.88	$C^{2,6}H$ 6.87; $C^{3,5}H$ 6.64
Asp	87	8.88	5.42	3.53, 2.62	
Thr	88	8.10	3.95	4.45	$C^{\gamma}H_3$ 1.33
Lys	89	8.19	4.50	2.02, 1.96	$C^{\gamma}H_2$ 1.41
Gly	90	8.25	4.23, 3.71		
Lys	91	8.70	4.31	1.85	
Asn	92	8.84	4.19	2.69, 2.52	
Val	93	8.65	4.12	2.03	$C^{\gamma}H_3$ 0.92, 0.77
Leu	94	7.17	4.30	1.56	$C^{\gamma}H$ 1.30; $C^{\delta}H_3$ 0.79, 0.57
Glu	95	8.19	5.32	1.97, 1.80	$C^{\gamma}H_2$ 2.26
Lys	96	8.51	4.61	1.48, 1.39	
Ile	97	8.05	5.25	1.62	$C^{\gamma}H_3$ 0.85; $C^{\gamma}H_2$ 1.01, 0.99; $C^{\delta}H_3$ 0.78
Phe	98	9.74	5.06	3.21, 2.91	$C^{2,6}H$ 7.38; $C^{3,5}H$ 7.33; $C^{4}H$ 7.30*
Asp	99	8.81	4.98	2.81, 2.19	
Leu	100	8.57	4.89	2.50	
Lys	101	8.54	4.43	1.00, 0.31	$C^{\gamma}H_2$ 0.91; $C^{\delta}H_2$ 1.31, 1.15; $C^{\epsilon}H_2$ 2.74
Ile	102	8.19	(4.75)	1.80	$C^{\gamma}H_3$ 0.74; $C^{\gamma}H_2$ 1.38, 1.08; $C^{\delta}H_3$ 0.64
Gln	103	8.86	4.66	2.15, 2.08	$C^{\gamma}H_2$ 2.34, $N^{\epsilon}H_2$ 7.23, 6.55
Glu	104	8.81	4.33	2.13, 2.00	$C^{\gamma}H_2$ 2.43, 2.35
Arg	105	7.92	4.19	1.84, 1.71	$C^{\gamma}H_2$ 1.55; $C^{\delta}H_2$ 3.15; $N^{\epsilon}H$ 7.17

[a] Chemical shifts are in parts per million (ppm) referenced to the water resonance, calibrated in turn at 4.631, 4.755, and 4.879 ppm at 37, 25, and 13 °C, respectively, on an external DSS standard and are accurate to ±0.01 ppm. Assignments mainly determined at 37 °C and at 13 °C are denoted in ( ) and [ ], respectively. [b] Resonances in the "others" column that are not labeled belong to the spin system, but the position in the side chain is not known. [c] Resonances marked with an asterisk are tentatively assigned.

In the two intersheet loops A–B and E–F connecting strand A with B and strand E with F, respectively, NOEs from residues His72 and Leu73 to residues Gly14 and Gln15 were observed. $C^{\alpha}H(i)/NH(i+3)$, $C^{\alpha}H(i+1)/NH(i+3)$, and consecutive strong sequential $NH(i)/NH(i+1)$ NOEs in the tetrapeptide segment Thr75–Asp76–Asp77–Gln78 indicate a 3_{10} helical turn in that part of the E–F loop. The same is true for the four-residue segment Thr38–Ser39–Asp40–Lys41 in the C–C′ loop. Residues Ile21–Phe24 and Lys57–Tyr60 form different types of reverse turns with Pro22 and Asp58 at position $i+1$, respectively. In the latter portion of this long B–C loop, a series of consecutive sequential $NH(i)/NH(i+1)$ NOEs was observed for the segment Ser27–Asp28–Asp29–Ile30–Asp31. Additionally, Ile30 and Asp31, which immediately precede the C strand show several long range NOEs to Asp87 and Thr88 at the end of the F strand. Likewise, in the loop between the F and G strand, $NH(i)/NH(i+1)$ connectivities were observed, although residues 92 and 93 also make contacts to residues 86 and 87 in the F strand. In the loop region between strands D and E, three consecutive $NH(i)/NH(i+1)$ NOEs, a very weak $C^{\alpha}H(64)/NH(67)$ NOE, and a $C^{\alpha}H(64)/NH(66)$ NOE were observed, indicating a reverse turn between residues 64 and 67. Note that the single *N*-linked glycosylation site of hu-$sCD2_{105}$is located at Asn65.

A significant number of NOEs between side chain resonances of residues of the two β-sheets have been observed. As a consequence, the side chain orientation of β-strand residues could be determined, because the side chains within a β-strand point alternatively above and below the β-sheet (see Figure 7). Most of these contacts occur between hydrophobic residues implying a hydrophobic core between the two sheets. For example, 41, 40, and 32 long-range NOEs have been identified for Phe98, Trp35, and Leu19, respectively. Therefore, it was possible to determine the approximate orientation of the two β-sheets and to build a model of hu-$sCD2_{105}$ in a late stage of the assignment work facilitating the identification of some yet ambiguous side chain resonances. Overall, the assignment of over 80% of all side chain ^1H resonances could unambiguously be achieved.

DISCUSSION

Detailed structural studies of glycoproteins by either NMR spectroscopy or X-ray crystallography are scarce, and we are unaware of any published NMR assignments of a glycoprotein containing an intact carbohydrate moiety that is required for its functional activity. We previously demonstrated that the high mannose *N*-glycan attached to Asn65 in hu-$sCD2_{105}$ is essential for its adhesion functions (Recny et al., 1992). However, it was unclear whether this single *N*-linked carbohydrate moiety serves only to stabilize the conformation of the amino-terminal CD58-binding domain, contributes to the recognition of CD58 as part of a ligand binding site, or both. In order to better understand the structural aspects that regulate human CD2 adhesion functions, we initiated the determination of the three-dimensional structure of human CD2 by NMR spectroscopy. For that purpose, we were required to utilize the intact glycosylated adhesion domain (hu-$sCD2_{105}$) which we derived from the entire extracellular two-domain CD2 segment (hu-$sCD2_{182}$) expressed in CHO cells. This molecule contains a single high mannose *N*-glycan composed of heterogeneous isomeric structures with variable branching patterns [$(Man)_nGlcNAc_2$, $n = 5–9$], which further complicates the process of assigning its ^1H resonances. Normally, NMR assignments for a protein of the size of hu-$sCD2_{105}$ can be greatly facilitated by isotopically labeling the protein *in vivo* with ^{15}N and ^{13}C amino acids if the protein can be functionally expressed in *Escherichia coli* (McIntosh & Dahlquist, 1990). This strategy has often proved successful

for glycoproteins that do not require intact carbohydrate chains for maintaining the structural and functional integrity of the glycoprotein, as is the case for rat CD2 (Driscoll et al., 1991). However, since *N*-glycosylation is critical for human CD2 adhesion functions, we could not take advantage of this strategy to assign the NMR resonances of the intact glycosylated adhesion domain of human CD2.

We have presented in this paper ^{1}H resonance assignments for almost all the residues in the adhesion domain of human CD2 (hu-sCD2$_{105}$). On the basis of qualitative analysis of NOE data obtained at three different temperatures (13, 25, and 37 °C), pH 4.5, with several mixing times (38, 76, 100, and 200 ms), the secondary structure and topology of hu-sCD2$_{105}$ have also been determined. NOESY and TOCSY spectra recorded at 25 °C and pH 7.0 revealed no obvious structural differences between hu-sCD2$_{105}$ samples analyzed at physiological pH compared to pH 4.5, suggesting that the protein structure remains largely unperturbed when the pH is lowered in order to obtain better NMR spectra. These studies reveal an overall structure consisting of nine β-sheets for hu-sCD2$_{105}$ arranged in a manner typical for Ig V domains (see Figure 8). In addition, a large number of NOEs were observed between hydrophobic residues of the two β-sheets, suggesting that a closely packed hydrophobic core is situated between the two sheets.

Except for Arg48, Glu56, and Lys57, all backbone ^{1}H resonances for the remaining 102 residues have unambiguously been assigned. These three residues lie within a region that appears to be significantly more mobile than the remainder of the protein, as many residues between Thr38 and Lys57 showed only weak or missing intraresidue cross peaks in the NOESY spectra. Consequently, the existence of the C″strand (residues 53–55) is based merely on two weak C$^\alpha$H(i)/C$^\alpha$H(j) interstrand NOEs observed between residues of strands C′ and C″ (see Figure 7b). However, two additional interstrand NOEs involving side chain ^{1}H resonances confirmed a proximity of residues within these two strands.

The assignments of side chain resonances as well as of the NH resonance could not be obtained for Arg48 that is located in the C′–C″ loop immediately following the C′ strand. Interestingly, we observe that clostripain does not cleave the Arg48–Lys49 peptide bond of hu-sCD2$_{105}$ under native conditions where the Arg105–Val106 and Arg146–Val147 peptide bonds are rapidly hydrolyzed. In fact, this unusual property has facilitated our preparation of intact adhesion domain from the two-domain molecule. Assuming that Arg48 is highly mobile and solvent exposed due to its location within the C′–C″ loop, one might predict it to be readily accessible to proteolytic attack by clostripain. However, hydrophobic contacts observed between residues of the two β-sheets suggest that the D–E loop, where the glycomer is attached at Asn65, is situated close to Arg48 (see Figure 8). Conceivably, the high mannose oligosaccharide could partially mask the accessibility of Arg48 and limit the binding of and subsequent cleavage by clostripain at this site. This hypothesis is supported by the additional observation that when the *N*-glycan is removed from hu-sCD2$_{105}$ by endoglycosidase digestion, the Arg48–Lys49 peptide bond is rapidly cleaved within minutes (M. Knoppers and M. Recny, unpublished results).

Despite the presence of the functionally important glycan in hu-sCD2$_{105}$, its secondary structure is similar to that of the unglycosylated rat analogue. However, detailed comparison of the secondary structure present in the adhesion domain of the NMR solution structure of the nonglycosylated rat CD2 domain 1 (r-sCD2$_{99}$) (Driscoll et al., 1991), the crystal structure of the entire extracellular region of rat CD2 (r-sCD2$_{177}$) (Jones et al., 1992) and hu-sCD2$_{105}$ reveals a number of differences (see Figure 8). The only structural features that are identical among all three molecules are the lengths of the A–B loop and the D strand. Hu-sCD2$_{105}$ is three residues longer than rat CD2 at the amino-terminus due to differences in the primary sequence and seems to form a kink at positions 5 and 6 with the four amino-terminal residues pointing away from the G strand. In r-sCD2$_{177}$ the A strand was found to be one residue longer than in the other two structures. Similar to r-sCD2$_{177}$, the B strand in hu-sCD2$_{105}$ appears to be one residue shorter than in r-sCD2$_{99}$. Although residues in the B–C loop are highly conserved between human and rat CD2, hu-sCD2$_{105}$ does not appear to form the distinctive kink observed in the rat structures within this loop. Hence, no internal side chain contacts between the loops connecting strands B to C and D to E have been observed in human CD2. This difference may be attributed to the presence of the glycan in hu-sCD2$_{105}$. Interestingly, the B–C loop in r-sCD2$_{177}$ is two residues shorter at the carboxy-terminal end such that the C strand starts two residues earlier than in the single domain structures of rat and human CD2. In hu-sCD2$_{105}$, the C–C′ loop is three and five residues longer than in r-sCD2$_{99}$ and r-sCD2$_{177}$, respectively. However, the sequence alignment of human CD2 and rat CD2 reveals two additional residues in the primary sequence of human CD2 within this loop (Driscoll et al., 1991). Because the backbone assignments for Arg48, Glu56, and Lys57 are still partially missing for hu-sCD2$_{105}$, the ends of the C′ strand and the C″ strand have not clearly been defined. However, the amino-terminus of the C′ strand in r-sCD2$_{99}$ and r-sCD2$_{177}$, respectively, is one and three residues longer than in hu-sCD2$_{105}$. The E strand in r-sCD2$_{99}$ starts one residue earlier than in hu-sCD2$_{105}$. Note that, for the human structure, this D–E loop is three residues long and contains the glycosylation site at Asn65. The E strand in r-sCD2$_{177}$ ends one sequence position before it ends in the single domain forms of CD2. The F strand of hu-sCD2$_{105}$ appears to be one residue shorter than in rat CD2 at both ends. In r-sCD2$_{177}$ the G strand starts two sequence positions earlier than in the other two forms. In r-sCD2$_{99}$ on the other hand, this strand ends one position before it ends in the other two structures. Consequently, the G strand is 12, 10, and 9 residues long for r-sCD2$_{177}$, hu-sCD2$_{105}$ and r-sCD2$_{99}$, respectively. Structure calculations for hu-sCD2$_{105}$, are currently under way that will show to what extent these differences in secondary structure among the three proteins are reflected in their three-dimensional structures.

Previous studies on human CD2 have shown that single mutations at sequence positions Lys43 and Ile44 (C–C′ loop), Ala45 and Gln46 (C′ strand), Lys82 and Tyr86 (F strand), Asp87 and Gly90 (F–G loop), and Leu94 (G strand) disrupt CD58 binding (Peterson & Seed, 1987; Wolff et al., 1990) (see Figure 8). According to the NOE contacts observed between hydrophobic residues of the two β-sheets, the side chains of Gln46, Lys82, and Tyr86 are solvent-exposed on the surface of the GFCC′C″-sheet (see Figure 7a). On the other hand, the side chains of Ala45 and Leu94 are oriented toward the hydrophobic core that is situated between the two β-sheets. In human CD2 the orientations of the side chains of Lys43, Ile44, and Asp87, have not been defined yet. However, in the case of Lys43 and Asp87 the side chains of the homologous residues in rat CD2 are solvent exposed in the rat structure. However, only calculated structures of hu-sCD2$_{105}$ will reveal the exact locations of these side chains in human CD2. Together with additional mutational studies, the three-

dimensional structure of hu-sCD2$_{105}$ will presumably lead to a better understanding of the binding surface provided by CD2 for the ligand, CD58.

Two NOE contacts between Gly90 in the F–G loop and one of the anomeric resonances of the oligosaccharide have tentatively been assigned, suggesting that some part of the high mannose glycan is situated close to this portion of the F–G loop. Clearly, this needs to be further investigated by an extension of the carbohydrate assignments, but glycoform heterogeneity combined with severe resonance overlap in the homonuclear NMR spectra have hampered complete assignments and conformational studies of the oligosaccharides thus far.

It is our belief that the assignments listed in Table I are the most complete possible using homonuclear 2D NMR methods and that further assignments will only be possible using heteronuclear-edited 3D NMR techniques. Recently, a fully ^{15}N and partially ^{13}C double-labeled hu-sCD2$_{105}$ sample was prepared by isotopic enrichment in CHO cells (Recny et al., manuscript in preparation). Analysis of this sample by heteronuclear-edited multidimensional NMR techniques will help to achieve further protein and carbohydrate assignments for hu-sCD2$_{105}$. This will be necessary to better define the functional importance of the glycan present in hu-sCD2$_{105}$ and better characterize the binding surface provided by human CD2 for binding of CD58. In addition, dynamical studies will be carried out to determine if weak and missing signals between Thr38 and Lys57 are due to a higher mobility of this part of the protein.

ACKNOWLEDGMENT

We thank Dr. A. Krezel for many helpful discussions and his support regarding computational matters. We also acknowledge Dr. M. Concino for advice on mammalian cell culture, K. Gordon, H. Stump, C. Tully, and J. Godoy for their technical assistance, and Dr. E. L. Reinherz for many helpful discussions.

SUPPLEMENTARY MATERIAL AVAILABLE

Sequence-specific assignments for residues 23–105. Different parts of the fingerprint region of the same spectrum as in Figure 3 showing sequential $d_{\alpha N}(i,i+1)$ connectivity pathways for residues (a) 58–64, 67–75, 78–88, and 94–99, (b) 22–37, and (c) 41–44 and 49–55. Part of the NH–NH region of a NOESY spectrum of hu-sCD2$_{105}$, recorded in H_2O at 25 °C, pH 4.5, with a mixing time of 76 ms, showing sequential connectivity pathways $d_{NN}(i,i+1)$ for segments where $C^{\alpha}H(i)$–$NH(i+1)$ cross peaks were weak or missing (7 pages). Ordering information is given on any current masthead page.

REFERENCES

Anil-Kumar, Ernst, R. R., & Wüthrich, K. (1980) *Biochem. Biophys. Res. Commun. 95*, 1–6.

Arulanandam, A. R. N., Moingeon, P., Concino, M. F., Recny, M. A., Kato, K., Yagita, H., Koyasu, S., & Reinherz, E. L. (1993) *J. Exp. Med. 177*, 1439–1450.

Bierer, B. E., Peterson, A., Barbosa, J., Seed, B., & Burakoff, S. J. (1988) *Proc. Natl. Acad. Sci. U.S.A. 85*, 1194–1198.

Bierer, B. E., Sleckman, B. P., Ratnofsky, S. E., & Burakoff, S. J. (1989) *Annu. Rev. Immunol. 7*, 579–599.

Braunschweiler, L., & Ernst, R. R. (1983) *J. Magn. Reson. 53*, 521–528.

Braunschweiler, L., Bodenhausen, G., & Ernst, R. R. (1983) *Mol. Phys. 48*, 535–569.

Brown, S. C., Weber, P. L. & Mueller, L. (1988) *J. Magn. Reson. 77*, 166–169.

Chang, H.-C., Moingeon, P., Lopez, P., Krasnow, H., Stebbins, C., & Reinherz, E. L. (1989) *J. Exp. Med. 169*, 2073–2083.

Chylla, R. A., & Markley, J. M. (1993) *J. Magn. Reson.* (in press).

Deckert, M., Kubar, J., Zoccola, D., Bernard-Pomier, G., Angelisova, P., Horejsi, V., & Bernard, A. (1992) *Eur. J. Immunol. 22*, 2943–2947.

Driscoll, P. C., Cyster, J. G., Campbell, I. D., & Williams, A. F. (1991) *Nature 353*, 762–765.

Dustin, M. L., & Springer, T. A. (1989) *Nature 341*, 619–624.

Eccles, C., Güntert, P., Billeter, M., & Wüthrich, K. (1991) *J. Biomol. NMR 1*, 111–130.

Hahn, W. C., Menu, E., Bothwell, A. L. M., Sims, P. J., & Bierer, B. E. (1992) *Science 256*, 1805–1807.

Jeener, J., Meier, B. H., Bachmann, P., & Ernst, R. R. (1979) *J. Chem. Phys. 71*, 4546–4553.

Jones, E. Y., Davis, S. J., Williams, A. F., Harlos, K., & Stuart D. I. (1992) *Nature 360*, 232–239.

Kato, K., Koyanagi, M., Okada, H., Takanashi, T., Wong, Y. W., Williams, A. F., Okumura, K., & Yagita, H. (1992) *J. Exp. Med. 176*, 1241–1249.

Killeen, N., Moessner, R., Arvieux, J., Willis, A., & Williams, A. F. (1988) *EMBO J. 7*, 3087–3091.

Koyasu, S., Lawton, T., Novick, D., Recny, M. A., Siliciano, R. F., Wallner, B. P., & Reinherz, E. L. (1990) *Proc. Natl. Acad. Sci. U.S.A. 87*, 2603–2607.

Marion, D., & Wüthrich, K. (1983) *Biochem. Biophys. Res. Commun. 113*, 967–974.

Marion, D., Ikura, M., & Bax, A. (1989) *J. Magn. Reson. 84*, 425–428.

McIntosh, L. P., & Dahlquist, F. W. (1990) *Q. Rev. Biophys. 23*, 1–38.

Meuer, S. C., Hussey, R. E., Fabbi, M., Fox, D., Acuto, O., Fitzgerald, K. A., Hodgdon, J. C., Protentis, J. P., Schlossman, S. F., & Reinherz, E. L. (1984) *Cell 36*, 897–906.

Moingeon, P., Chang, H.-C., Sayre, P. H., Clayton, L. K., Alcover, A., Gardner, P., & Reinherz, E. L. (1989a) *Immunol. Rev. 111*, 111–144.

Moingeon, P., Chang, H.-C., Wallner, B. P., Stebbins, C., Frey, A. Z., & Reinherz E. L. (1989b) *Nature 339*, 312–314.

Moingeon, P. E., Lucich, J. L., Stebbins, C. C., Recny, M. A., Wallner, B. P., Koyasu, S., & Reinherz, E. L. (1991) *Eur. J. Immunol. 21*, 605–610.

Mueller, L. (1979) *J. Am. Chem. Soc. 101*, 4481–4484.

Otting, G., & Wüthrich, K. (1990) *Q. Rev. Biophys. 23*, 39–96.

Otting, G., Senn, H., Wagner, G., & Wüthrich, K. (1986) *J. Magn. Reson. 70*, 500–505.

Peterson, A., & Seed, B. (1987) *Nature 329*, 842–846.

Piantini, U., Sørensen, O. W., & Ernst, R. R. (1982) *J. Am. Chem. Soc. 104*, 6800–6801.

Rabin, E. R., Gordon, K., Knoppers, M. H., Luther, M. A., Neidhardt, E. A., Flynn, J. F., Sardonini, C. A., Sampo, T. M., Concino, M. F., Recny, M. A., Reinherz, E. L., & Dwyer, D. S. (1993) *Cell. Immunol. 149*, 24–38.

Rance, M., Sørensen, O. W., Bodenhausen, G., Wagner, G., Ernst, R. R., & Wüthrich, K. (1983) *Biochem. Biophys. Res. Commun. 117*, 479–485.

Recny, M. A., Neidhardt, E. A., Sayre, P. H., Ciardelli, T. L., & Reinherz, E. L. (1990) *J. Biol. Chem. 265*, 8542–8549.

Recny, M. A., Luther, M. A., Knoppers, M. H., Neidhardt, E. A., Khandekar, S. S., Concino, M. F., Schimke, P. A., Francis, M. A., Moebius, U., Reinhold, B. B., Reinhold, V. N., & Reinherz, E. L. (1992) *J. Biol. Chem. 267*, 22428–22434.

Sayre, P. H., Chang, H.-C., Hussey, R. E., Brown, N. R., Richardson, N. E., Spagnoli, G., Clayton, L. K., & Reinherz, E. L. (1987) *Proc. Natl. Acad. Sci. U.S.A. 84*, 2941–2945.

Sayre, P. H., Hussey, R. E., Chang, H.-C., Ciardelli, T. L., & Reinherz, E. L. (1989) *J. Exp. Med. 169*, 995–1009.

Selvaraj, P., Plunkett, M. L., Dustin, M., Sanders, M. E., Shaw,

S., & Springer, T. A. (1987) *Nature 326*, 400–403.
Sewell, W. A., Brown, M. H., Dunne, J., Owen, M. J., & Crumpton, M. J. (1986) *Proc. Natl. Acad. Sci. U.S.A. 83*, 8718–8722.
Shaka, A. J., & Freeman, R. (1983) *J. Magn. Reson. 51*, 169–173.
Shaka, A. J., Lee, C. J., & Pines, A. (1988) *J. Magn. Reson. 77*, 274–293.
Shaw, S., Ginther Luce, G. E., Quinones, R., Gress, R. E., Springer, T. A., & Sanders, M. E. (1986) *Nature 323*, 262–264.
Wagner, G. (1990) *Prog. Nucl. Magn. Reson. Spectrosc. 22*, 101–139.
Wagner, G., & Wüthrich, K. (1982) *J. Mol. Biol. 155*, 347–366.
Wagner, G., & Zuiderweg, E. R. P. (1983) *Biochem. Biophys. Res. Commun. 113*, 854–860.
Williams, A. F., & Barclay A. N. (1988) *Annu. Rev. Immunol. 6*, 381–406.
Williams, A. F., Davis, S. J., He, Q., & Barclay A. N. (1989) *Cold Spring Harbor Symp. Quant. Biol. 54(2)*, 637–647.
Wolff, H. L., Burakoff, S. J., & Bierer, B. E. (1990) *J. Immunol. 144*, 1215–1220.
Wong, Y. W., Williams, A. F., Kingsmore, S. F., & Seldin, M. F. (1990) *J. Exp. Med. 171*, 2115–2130.
Wüthrich, K. (1986) *NMR of Proteins and Nucleic Acids*, John Wiley, New York.